https://doi.org/10.48048/tis.2024.7657

Structural, Energetic, and Electronic Properties of H-Interstitial in C-Monovacancy: A First-Principles Density Functional Theory

Nurul Fajariah[1], Malika Fadlliyanai[1], Diki Purnawati[1], Harmon Prayogi[2], Ari Dwi Nugraheni[1] and Sholihun Sholihun[1,*]

[1]Department of Physics, Faculty of Mathematics and Natural Sciences, Universitas Gadjah Mada, Yogyakarta 55281, Indonesia
[2]Department of Data Science, Faculty of Mathematics and Natural Sciences, Universitas Negeri Surabaya, Surabaya 60231, Indonesia

([*]Corresponding author's e-mail: sholihun@ugm.ac.id)

Received: 27 October 2023, Revised: 20 November 2023, Accepted: 27 November 2023, Published: 30 April 2024

Abstract

We discover a unique structural-modified diamond that exhibits similar symmetry and band gap energy to that of the pure diamond. We study a complex carbon-vacancy-hydrogen in the diamond using the density-functional-theory method. The defective models are created by adding H-interstitial (H_i, where i = 1, 2, 3 and 4) in the 3D diamond C-monovacancy. The result shows that carbon-vacancy-hydrogen defects significantly decreased the symmetry from T_d to C_{2V}. Likewise, the volumetric size of the systems is widening up to 48.70 %, while the optimized band gap energies are narrowing. Additional states appeared in the C-monovacancy, H_1-V, H_2-V, and H_3-V systems which further improved electron mobility. The H_i compensates the C-monovacancy which further serves as a deep donor. Interestingly, H_4-V exhibits similar symmetry and band gap energy to that of the pure diamond, but its volumetric size is 48.70 % wider.

Keywords: C-monovacancy, H-interstitial, Formation energy, Reaction coordinate, Band structure

Introduction

Over decades, diamond has gained a huge interest in both experimental [1,2] and computational [3-5] studies. Diamond is a unique semiconductor material with an ultra-wide band gap energy (5.47 eV) and superb electronic as well as optical properties [6]. Diamond holds potential application in high-technology areas due to its high electron-hole mobilities [7], excellent thermal conductivity, and high breakdown voltage [8]. For that reason, diamond has been used for a wide range of applications, from electronic devices to industrial tools. Nevertheless, these superb properties are extremely sensitive to the presence of defects including impurities [9], vacancies [10] and doping [5,9]. One of the most common defects in the diamond material is vacancies. In many cases, the presence of vacancies has significantly affected the electronic, mechanical and optical properties of the diamond [10-12].

Density functional theory (DFT) has been established as a simulation approach to evaluate the properties of various vacancies materials such as diamond [10,13], graphene [14,15], germanene [16,17], germanium [18,19] and h-BN [20,21]. In our previous study, we successfully evaluated the multi-vacancies behavior of 3D diamond material. Multi-vacancies are large-sized vacancies which is formed by the diffusion of small-sized vacancies. Our calculation revealed that the C-vacancies distorted the atomic distances which further lowered the structural symmetries [10].

Aside from vacancies, hydrogen is also known as a ubiquitous defect in most semiconductor materials [22], particularly diamond [5,9]. The studies of hydrogen in diamonds have been widely investigated using various theoretical methods [9,23-25]. Hydrogen might be present as an interstitial defect which is located at the center bond site of carbon atoms in the diamond lattice [23,24]. Interestingly, these interstitial hydrogen (H_i) defects induced some defect states in the band gap which further compensated n-type and *p*-type dopants [23-25]. Nonetheless, there is still limited study that comprehensively studies the geometric, energetic and electronic properties of H-interstitial in diamond C-monovacancy.

Herein, this work aims to elucidate the effect of the structural, energetic, and electronic properties of the H-interstitial in C-multivacancy diamond. We modeled complex carbon-vacancy-hydrogen systems and evaluated the properties through DFT calculations. We evaluate the equilibrium geometry, symmetry, formation and absorption energies, reaction coordinates, and band structure of each defect system. We believe that the results will be beneficial for future development of diamond-based devices.

Materials and methods

The research uses the concept of continuous calculation. The basis of our computational approach is based on the plane-wave method, which is commonly used to investigate properties associated with defects and/or impurities in the 3D crystalline structure using Density Functional Theory (DFT) [4,5,10]. The code library used is PHASE/0 [20] and the Exchange Correlation Potential used to calculate is called Generalized Gradient Approximation (GGA) [4,10,26]. We use the ultrasoft-pseudopotential. The calculated lattice constant is obtained from optimizing the cell volume with respect to energy by using the Birch-Murnaghan equation of state defined as follows [27]:

$$G(V) = G_0 + \frac{9}{16} V_0 Q_0 \left\{ \left[\left(\frac{V_0}{V} \right)^{\frac{2}{3}} - 1 \right]^3 Q_0' + \left[\left(\frac{V_0}{V} \right)^{\frac{2}{3}} - 1 \right]^2 \left[6 - 4 \left(\frac{V_0}{V} \right)^{\frac{2}{3}} \right] \right\} \quad (1)$$

where G_0 is the minimum energy, V_0 is the optimized cell volume, Q_0 is the optimal bulk modulus and Q_0' is the gradient of the bulk modulus. Using Eq. (1), the optimized lattice constant is obtained to be 3.59 Å, which is close to the theoretical [28,29] and experimental [30-32] values.

The diamond supercell is modeled in a simple cubic supercell of 216 atoms. A cut-off energy of 25 Ry and a Monkhorst-Pack scheme with 4×4×4 k-points have been used for integration in the Brillouin zone. The geometry has been optimized for the relaxation of 216 atoms so that the atomic force is less than 5.0×10^{-3} eV Å^{-1}. The converged energy criterion is 10^{-6} hartree. We simulate the monovacancy defect by removing a carbon atom at the center of the supercell, resulting in C-monovacancy. Furthermore, 4 1st-nearest-neighbor atoms lose their bonds, resulting in 4 broken bonds of C atoms. The hydrogen interstitials were placed in each broken bond to create complex carbon-vacancy-hydrogen systems. The number of hydrogens varied from 1 to 4, following the number of broken bonds. Eventually, the configurations were denoted as H_1-V, H_2-V, H_3-V and H_4-V as shown in **Figures 1(c) - 1(f)**.

In particular, the atoms of C-monovacancy have similar forms as an irregular tetrahedron as displayed in **Figure 1(b)**. The defect volume and its change for each system are calculated using the following equation [33]:

$$V_{ir} = \frac{(4D^2E^2F^2 - D^2D'^2 - E^2E'^2 - F^2F'^2 - D'E'F')^{\frac{1}{2}}}{12} \quad (2)$$

where $D' = E^2 + F^2 - A^2$, $E' = D^2 + F^2 - B^2$, and $F' = D^2 + E^2 - C^2$. Moreover, the defect volume is calculated before modification/pure diamond (V_0) and after modification by carbon-vacancy-hydrogen (V_f). The volume changes before and after relaxation (ΔV) is calculated by the following equation [34]:

$$\Delta V = \frac{V_f - V_0}{V_0} \times 100\ \% \quad (3)$$

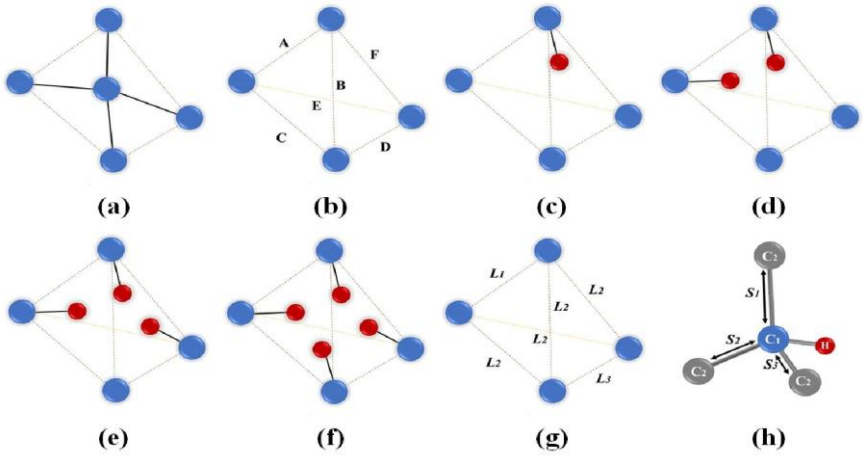

Figure 1 Schematic configurations of the (a) pure diamond, (b) C-monovacancy, (c) H_1-V, (d) H_2-V, (e) H_3-V, (f) H_4-V, (g) 1st-nearest-neighboring atoms, and (h) 2nd-nearest-neighboring atoms of C-monovacancy.

We also calculate the formation energies for each defect structure by using equations as follows [26]:

$$E_f = E_{sys} - (E_p - \mu_c + n\mu_H) \quad (4)$$

where E_f is the system formation energy (eV), is the system energy (eV), E_{sys} is the pure diamond system energy (eV), μ_c is the chemical potential of carbon atoms, μ_H is the chemical potential of hydrogen atoms and n is the number of hydrogen atoms. The energy of formation can provide us with information about the stability of a system.

In addition, we also calculated the absorption energy of each system. Absorption energy indicates the strength of the C-H bond interaction when the C-monovalent has hydrogen interstitials using the equation as follows [35,36].

$$E_a = E_{sys} - (E_v + n\mu_H) \quad (5)$$

where E_a is the absorption energy of the system (eV), E_{sys} is the energy of the system (eV), E_v is the monovacancy energy of diamond (eV), μ_H is the chemical potential of hydrogen atoms and n is the number of hydrogen atoms.

Results and discussion

Optimized geometry

We model the H-interstitial on C-monovacancy diamond as illustrated in **Figure 1**. The C atoms in pure diamond are uniformly separated at 2.54 Å apart (**Figure 1(a)**). Moreover, the C-monovacancy is created by removing a single C atom at the center of a 3D diamond (216 atoms) as shown in **Figure 1(b)**. In consequence, 4 dangling bonds are present at the 1st-nearest-neighboring atoms. While quadruple C atoms at the 2nd-nearest-neighboring atoms remained. As the geometry was optimized, it changed from a regular tetrahedron to an irregular tetrahedron. To further evaluate the volume-system changes, we measure the distance between the 1st-nearest-neighboring atoms (**Figure 1(g)**) and the 2nd-nearest-neighboring atoms (**Figure 1(h)**) of the optimized system. In the case of C-monovacancy, we obtain the 1st-nearest-neighboring distances of L_1 = 2.60 Å, L_2 = 2.74 Å and L_3 = 2.74 Å. While the 2nd-nearest-neighboring distances are S_1 = 1.56 Å, $S_2 = S_3$ 1.50 Å.

Interestingly, as the H-interstitial was added into the system to create H_1-V, the 1st-nearest-neighboring distances were changed to be L_1 = 2.78, L_2 = 2.78 Å and L_3 = 2.74 Å (**Figure 1(c)**). The system is widening by 10^{-2} Å relative to the C-monovacancy systems. The H atom tends to occupy the interstitial C – C and widen the systems since it needs an extra site for the H atom. Unlike the C-monovacancy, the H_1-V system has 1 H-site and 3 vacancy sites at the 2nd-nearest-neighboring site. Consequently, the 2nd-nearest-neighboring distances at the vacancy site are S_1 = 1.52 Å, $S_2 = S_3$ 1.49 Å. Surprisingly, the 2nd-nearest-neighboring distances at the H-site have similar atomic distances of $S_1 = S_2 = S_3$ = 1.52 Å.

Adding 2 H atoms to create the H_2-V system causes the 1st-nearest-neighboring distances to significantly change (**Figure 1(d)**). The L_1 and L_2 move 2.80 Å away, while the L_3 move 2.67 Å closer. The 2nd-nearest-neighboring distances at the vacancy site were also changed. The S_1 moves 1.55 Å away, whereas the S_2 and S_3 remained at 1.49 Å. As for the H_3-V system, the measured 1st-nearest-neighboring distances are L_1 = 2.85 Å, L_2 = 2.81 Å, and L_3 = 2.82 Å which is wider than the previous systems (C-monovacancy, H_1-V and H_2-V). The 2nd-nearest-neighboring distances at the vacancy site are $S_1 = S_2 = S_3$ 1.50 Å (**Figure 1(e)**). More importantly, the 2nd-nearest-neighboring distances at H-site are similar for H_1-V, H_2-V, and H_3-V which are $S_1 = S_2 = S_3$ = 1.52 Å and the C-H bond distances are 1.05 Å. The obtained C-H bond distance is close to the previous work [5,37]. Likely, as the H atom is bound to the triple C atoms, the systems are relaxed and optimize their distances to form C_3H where the distances are uniform.

In particular, for H_4-V, all C neighboring atoms are bound to H atoms. Resulting there are only the 2nd-nearest-neighboring distances at H-site which are $S_1 = S_2 = S_3$ = 1.52 Å. Interestingly, the 1st-nearest-neighboring distances are also uniform at $L_1 = L_2 = L_3$ = 2.89 Å which is wider than the other systems. From the explanation above, it can be inferred that the system tends to widen as the systems are modified by the complex carbon-vacancy-hydrogen systems. The changes in the system volume are summarized in **Table 1**.

Table 1 Summary of the atomic distances around the carbon-vacancy-hydrogen.

Systems	The 1st nearest neighbor			The 2nd nearest neighbor		
				Vacancy-site		H-site
	L_1 (Å)	L_2 (Å)	L_3 (Å)	S_1 (Å)	$S_2 = S_3$ (Å)	$S_1 = S_2 = S_3$(Å)
Pure	2.54	-	-	-	-	-
C-mono	2.60	2.74	2.74	1.56	1.50	-
H_1-V	2.78	2.78	2.74	1.52	1.49	1.52
H_2-V	2.80	2.80	2.67	1.55	1.49	1.52
H_3-V	2.85	2.81	2.81	1.50	1.50	1.52
H_4-V	2.89	2.89	2.89	-	-	1.52

Energetic and geometric evolution

We calculate the formation energies using Eq. (4). The formation energy of C-monovacancy is 6.75 eV which is in line with previous studies [4,10]. The C-monovacancy system is distorted, widening by 18.65 % and lowering the symmetry from T_d to D_{2d} [10,38,39] as summarized in **Table 2**. In the case of H_1-V, the formation energy is significantly decreased from 6.75 to 3.54 eV. The addition of 1 H atom to the C-monovacancy system results in a significant change in the unity of the system. To further elucidate the stages of change in the system, we plot the reaction coordinate as given in **Figure 2**.

The reaction coordinate represents the energetic and geometric evolution of the H-interstitial. In general, the reaction coordinate of the H1-V system consists of 4 states: C-monovacancy, initial state, transition state and final state. In the beginning, C-monovacancy has D_{2d} symmetry with the 1st-nearing-neighboring distances represented as L_1, L_2 and L_3. At the initial state, the 1st-nearest-neighboring atoms are remaining the same. Thereafter, at the transition state, the nearest atoms move away, increasing the distance. Eventually, the distance became wider and the system relaxed at the final state. It was widening by 28.50 % relative to the pure diamond. An outward relaxation occurs in the H_1-V system, resulting in the lowering symmetry from D_{2d} (C-monovacancy) to C_{3v} (H_1-V). The H_1-V has symmetry elements of C_3, $C_3^{2,}$ and σ_v as illustrated by **Figure 6(a)**.

Table 2 The calculated formation energies (E_f), absorption energies (E_a), volume of the optimized system (V), volume changes (ΔV), and symmetries of each configuration.

Systems	E_f (eV)	E_a (eV)	V (Å^3)	ΔV (%)	Symmetry	References
Pure	-	-	1.93	-	T_d	This work
	-	-	-	-	T_d	[10]
C-mono	6.75	-	2.29	18.65	D_{2d}	This work
	6.44	-	-	-	D_{2d}	[38]
	6.99	-	-	-	D_{2d}	[39]
H_1-V	3.54	–1.17	2.48	28.50	C_{3v}	This work
	-	-	-	-	C_{3v}	[37]
H_2-V	0.55	–2.12	2.54	31.61	C_{2v}	This work
H_3-V	–1.71	–2.33	2.68	38.86	C_{3v}	This work
H_4-V	–3.94	–2.52	2.87	48.70	T_d	This work

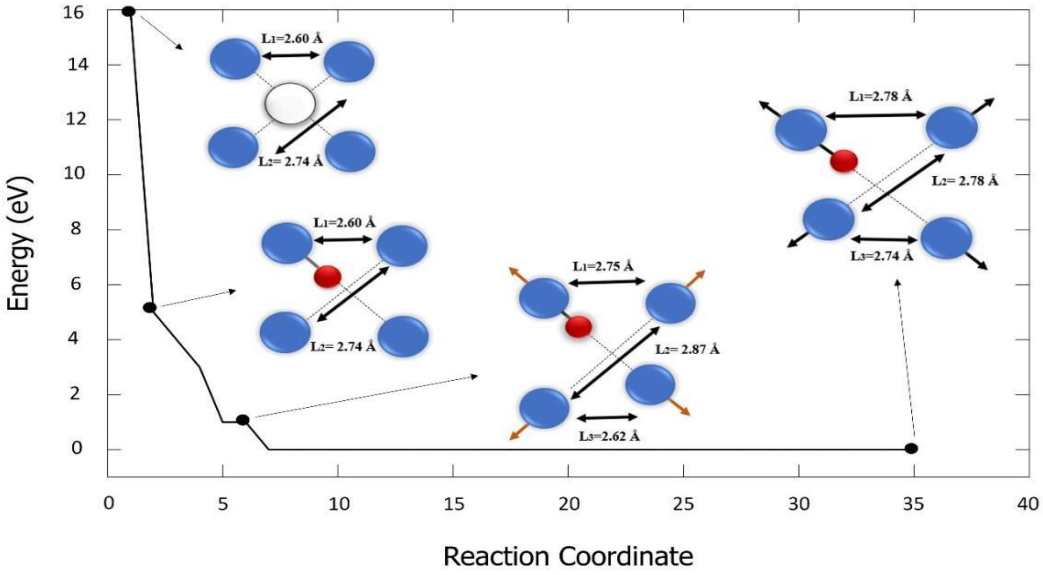

Figure 2 Reaction coordinate of H_1-V: An outward relaxation occurs and forms the C_{3V} symmetry configuration.

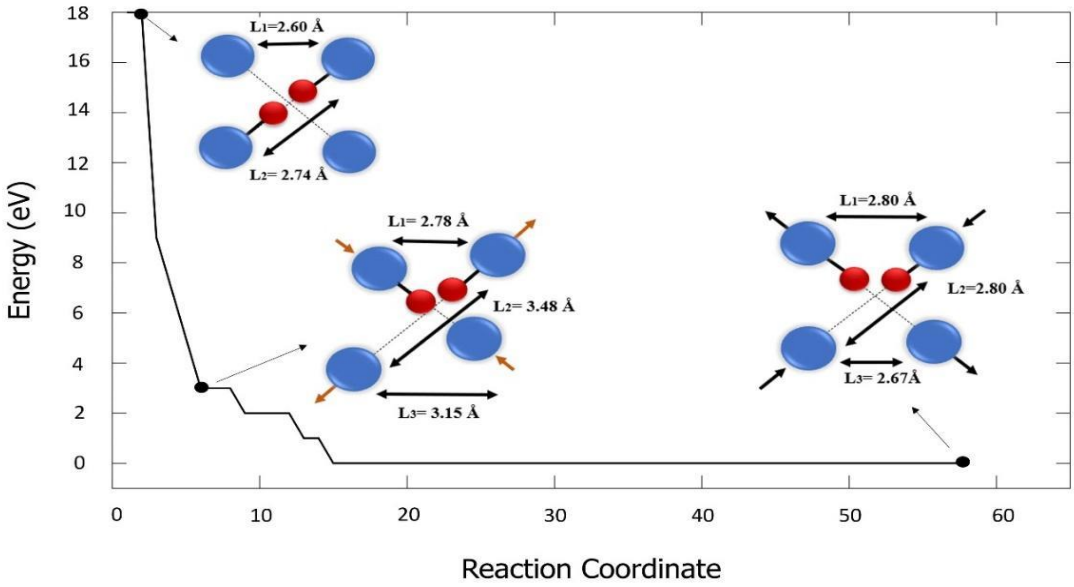

Figure 3 Reaction coordinate of H_2-V: An outward relaxation occurs and forms the C_{2V} symmetry configuration.

Moreover, the formation energy of H_2-V greatly decreased to 0.55 eV. It decreased by 2.99 eV relative to the H_1-V and 6.20 eV relative to the C-monovacancy system. **Figure 3** shows the reaction coordinate for the H_2-V system which only consists of 3 states. At the initial state, the nearest atoms have no change in distance. At the transition state, some of the nearest atoms are distanced, while other atoms become closer. In contrast, the atoms move oppositely at the final state. Thus overall, the system is outwardly relaxed with a volume growth of 31.61 %. In addition, the H_2-V has C_2 (rotation by p^2) in x-, y-, and z-axes, vertical mirrors in y-z-axes (σ_v) as well as in y-z-axes (σ'_v), as illustrated by **Figure 6(b)**. Therefore, it belongs to the C_{2v} symmetry which is lower than C-monovacancy and the H_1-V system.

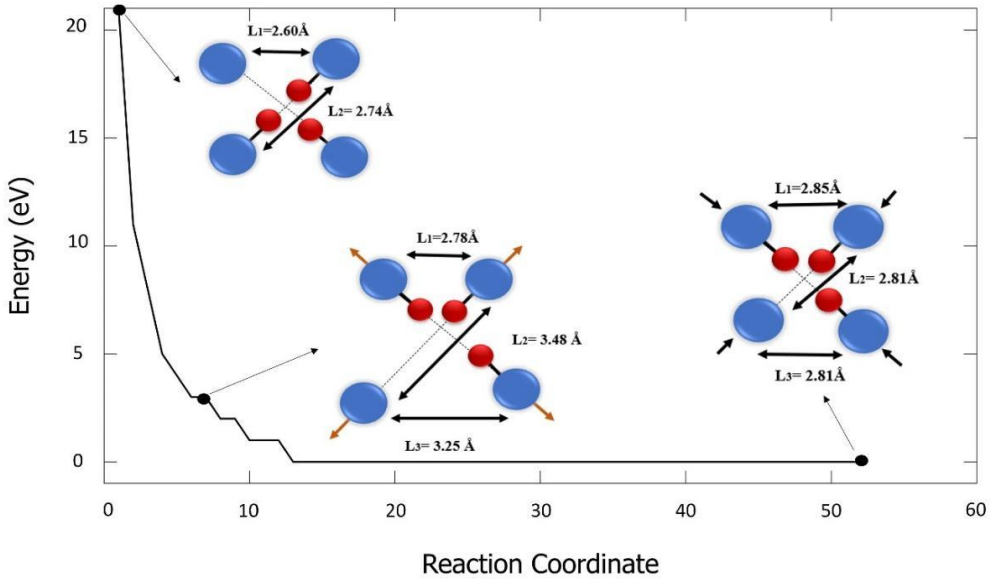

Figure 4 Reaction coordinate of H_3-V: An outward relaxation occurs and forms the C_{3V} symmetry configuration.

We next calculate the formation energy of the H_3-V system. It is also reduced by 2.26 eV compared to H_2-V and 8.46 eV from the C-monovacancy system. From **Figure 4**, we observe the initial, transition, and final states of the system during the relaxation process to track the changes in the distance between neighboring atoms. There is no change in the distance between nearby atoms at the initial state. Whereas at the transition state, the distance of the nearest atoms lengthens. Otherwise, in the final state, the distance of the nearest neighbors shortens. However, when compared to the initial state, the system still experiences expansion and volume growth, which is 38.86 % relative to the pure diamond. Similar to the H_1-V system, the H_3-V system has a C_{3v} symmetry with the axis of rotation passing through the dangling bond carbon and towards the vacancy center as illustrated in **Figure 6(c)**. Nevertheless, although H_1-V and H_3-V have similar symmetries, they are completely different in size. The H_3-V has a larger volume compared to the H_1-V system.

We subsequently added 4 H atoms into the C-monovacancy system to create the H_4-V system. The formation energy of the H_4-V system is –3.94 eV. A low formation energy value indicates that the system has good stability. The hydrogen atoms passivate the dangling bonds at the C-monovacancy, so there are no dangling bonds at the vacancy site. Then, by plotting the reaction coordinates, we analyze the changes in the system, refer to **Figure 5**. The distance between the closest atoms increases during the transition stage. Besides, the distance between nearest neighbors shortens and the atoms grow closer in the final state. However, when compared to the pure diamond, the system continues to expand and rise in volume by 48.70 %, which is referred to as outward relaxation. Interestingly, although these systems exhibit distinctive volume sizes, they have similar symmetries. The symmetry of the H_4-V system returns to that of pure diamond, which is T_d (**Figure 6(d)**). This is likely because all the broken bonds bind to H atoms, meaning there was no monovacancy in the diamond.

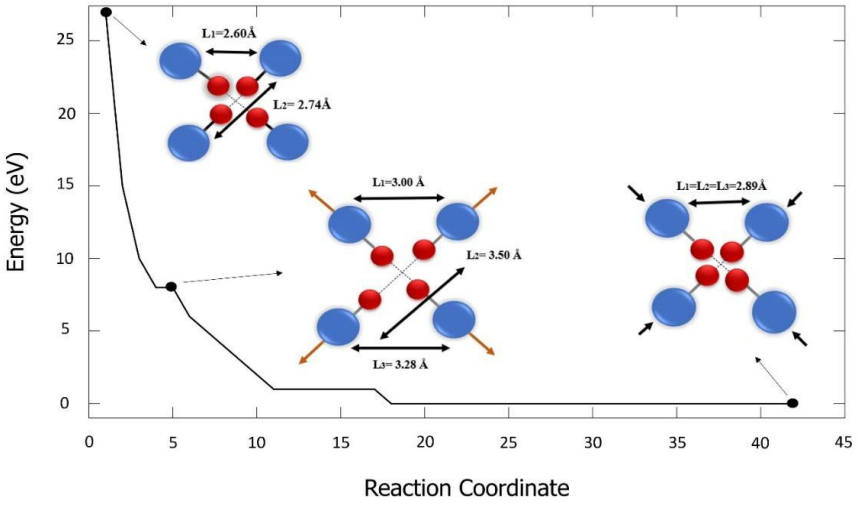

Figure 5 Reaction coordinate of H_4-V: An outward relaxation occurs and forms the T_d symmetry configuration.

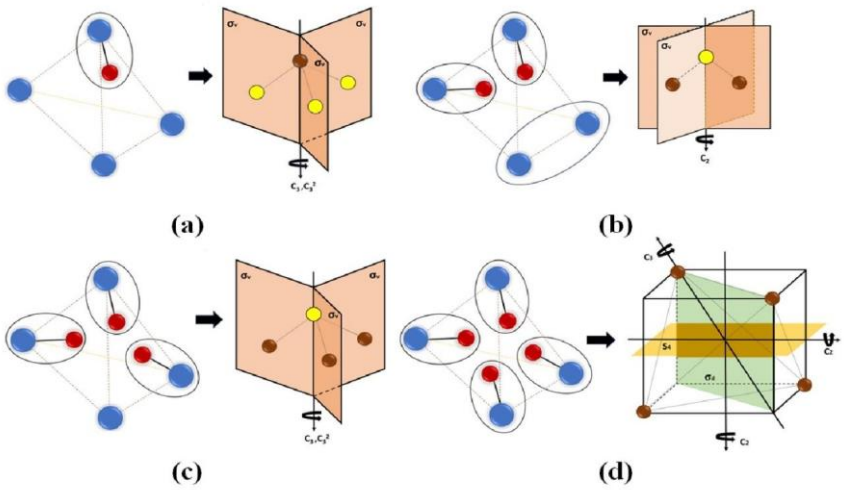

Figure 6 Schematic geometry of (a) C_{3V} symmetry for H_1-V, (b) C_{2V} symmetry for H_2-V, (c) C_{3V} symmetry for H_3-V, and (d) T_d symmetry for H_4-V system.

The formation energy describes the energy required to form the H_i-V system. It indicates the stability of a system [38-41]. The lower the formation energy, the more stable the system. The data trend shows that as the number of H atoms goes up, the formation energy decreases. From the data, we know that the H_4-V system is the most stable over the other systems. While the absorption energy represents the ability of H atoms to interact with carbon atoms in diamond. The strength of the C-H bond can be determined by calculating the absorption energy. Absorption energy of the H_1-V, H_2-V, H_3-V and H_4-V systems are shown in **Table 2**. The data supports the assertion that the H_4-V is the most stable system. It is characterized by its most negative energy absorption, meaning that the electrons' hydrogen atoms have absorbed energy and moved to a higher energy level, so the interaction is even stronger.

Band structure

We evaluate the band gap energy of each system by calculating the band structure as well as the DOS. **Figure 7** shows the resultant electronic band structure of pure diamond obtained from the DFT calculations. The band gap of each system is summarized in **Table 3**. From the calculation, the band gap value of pure diamond is 3.90 eV which agrees with the theoretical values [42,43]. It needs to be highlighted that the calculation through DFT (LDA or GGA) underestimates the band gap in most cases, as summarized in

Table 3. Therefore, the band gap values of the theoretical calculation will significantly differ from the experimental calculation [42-45].

Table 3 Summary of band gap of each system.

Systems	Method	Band gap (eV)	References
Pure diamond	GGA	3.90	This work
	LDA/GGA	3.27 - 4.11	[42]
	GGA	4.21	[43]
	HSE06	5.42	[43]
	GW	4.89-5.44	[42]
	GW	5.41-5.55	[44]
	Expt.	5.48	[45]
C-monovacancy	GGA	3.32	This work
H_1-V	GGA	3.45	This work
H_2-V	GGA	3.33	This work
	GGA	3.10	[46]
H_3-V	GGA	3.54	This work
H_4-V	GGA	3.90	This work

Figure 8 is the band structure and the DOS for the C-monovacancy system. The absence of a C atom tends to decrease the band gap energy from 3.90 to 3.32 eV. Moreover, it can be seen from **Figure 8** that the valence energy (E_v) is 1.12 eV above the valence band maximum (VBM), while the conduction energy (E_c) is 2.04 eV below the conduction band minimum (CBM). Thus, the actual band gap of C-monovacancy is 0.16 eV. Removing a single C atom induced a defect in the pure diamond which modified the band structure. The presence of vacancy tends to decrease the deformation potential constant which further increases the electron mobility [47].

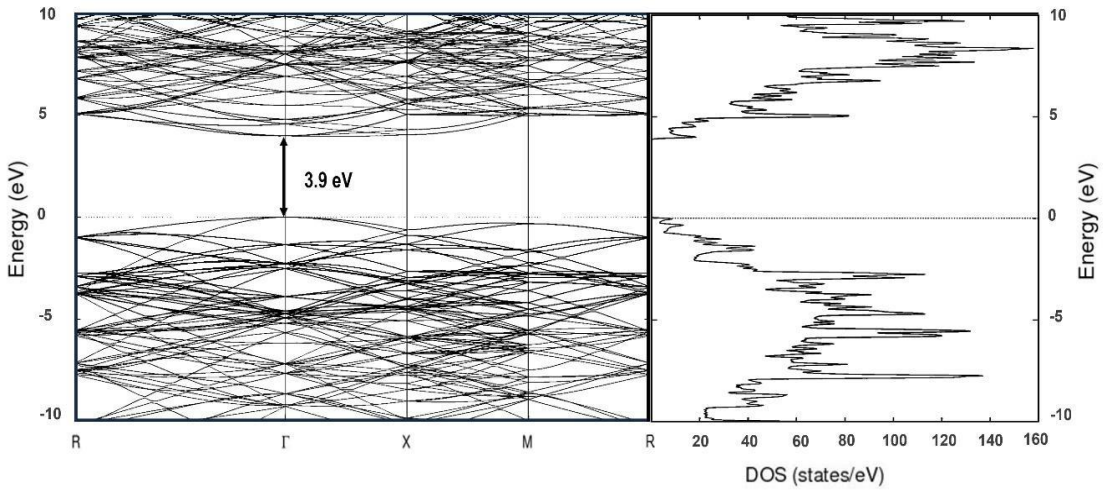

Figure 7 Band structure of the pure diamond.

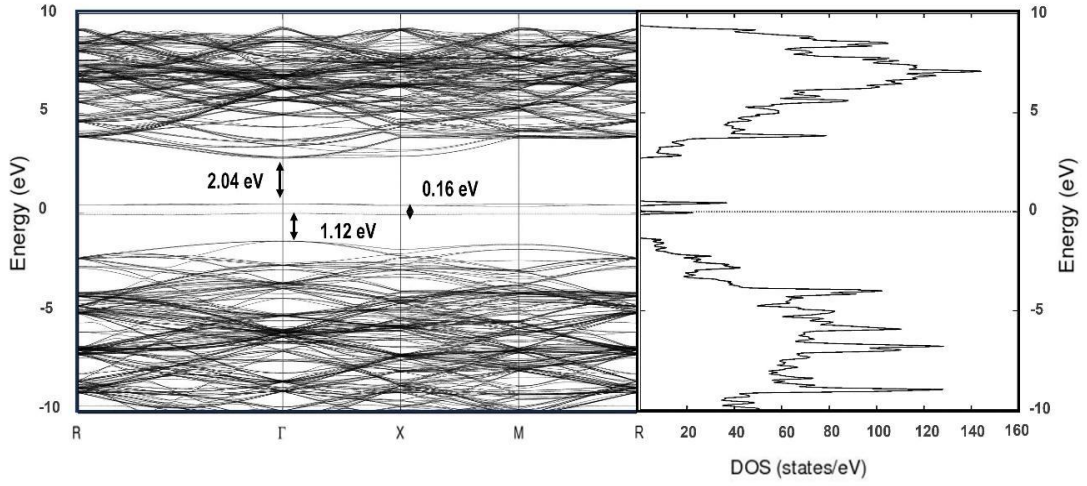

Figure 8 Band structure of the C-monovacancy diamond.

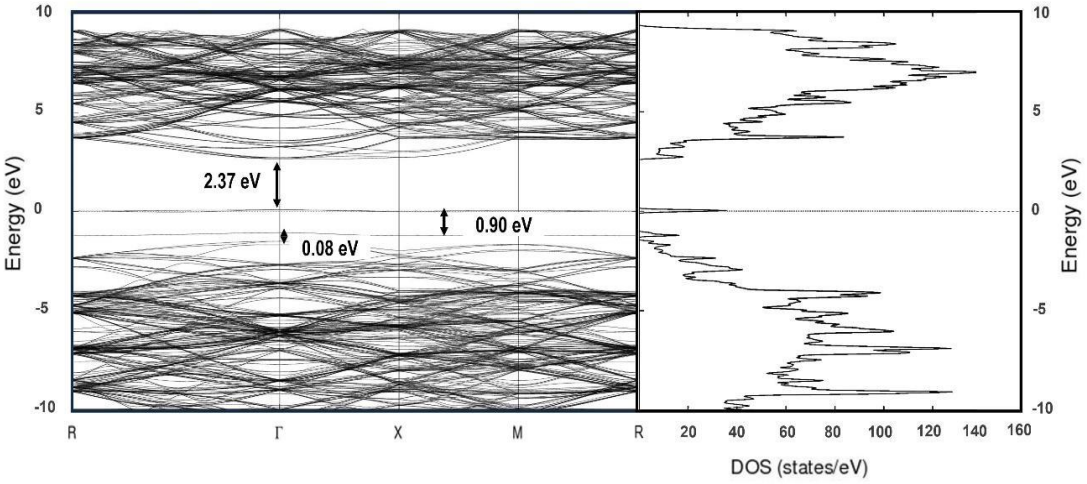

Figure 9 Band structure of the H_1-V system.

The band structure and the DOS for the H_1-V system is shown in **Figure 9**. The band gap of this system is 3.45 eV. Nevertheless, 2 additional states appeared near the Fermi level. As a single H atom was added into C-monovacancy, the E_c shifted closer to the Fermi level. In contrast, the E_v shifted closer to the VBM. In this case, the E_c is 2.37 eV below the CBM, and the E_v is 0.08 eV above the VBM. Therefore, the actual band gap of the H1-V system is 0.90 eV.

Figure 10 shows the band structure and DOS of the H_2-V system. Adding 2 H atoms shifted the E_c even closer to the Fermi level. The E_c is 2.53 eV below the CBM. By considering that the E_v is 0.16 eV above the VBM, we obtain the actual band gap of the H2-V system is 0.54 eV. As for the H_3-V system, the band structure and DOS can be seen in **Figure 11**. Similar to the H_2-V system, the presence of H-interstitial tends to shift the E_c way closer to the Fermi level.

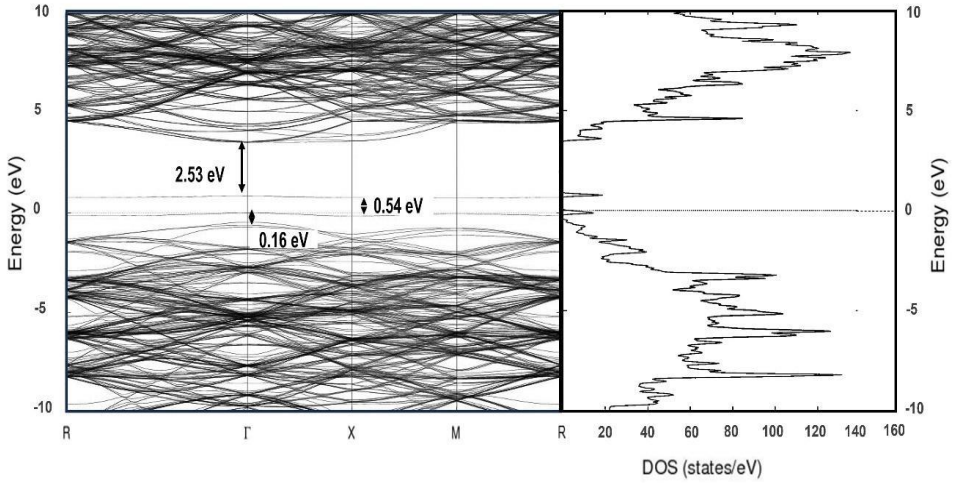

Figure 10 Band structure of the H_2-V system.

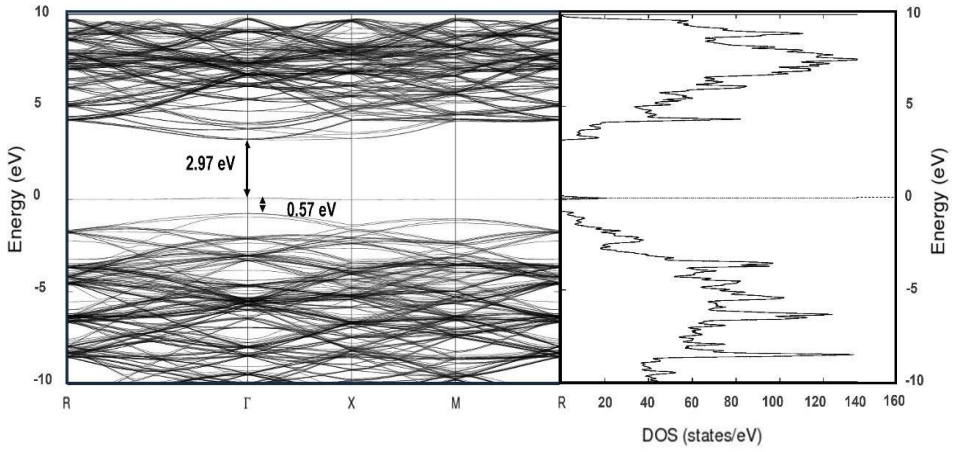

Figure 11 Band structure of the H_3-V system.

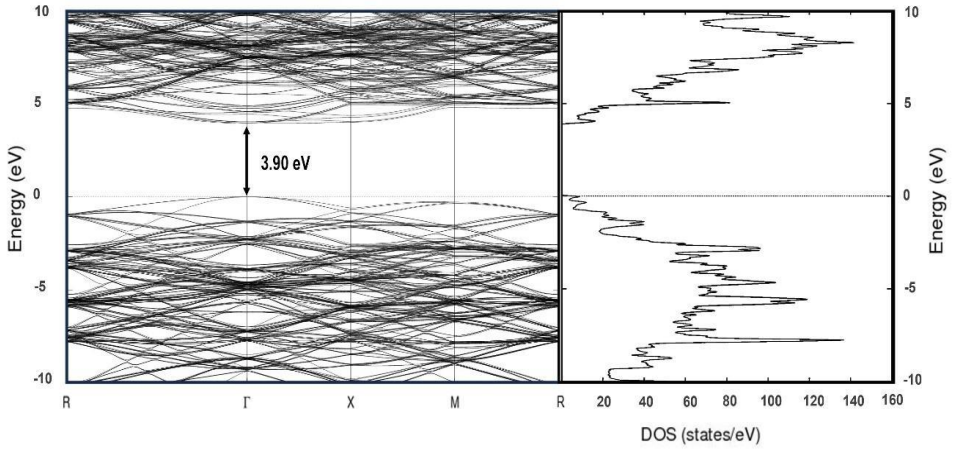

Figure 12 Band structure of the H_4-V system.

From **Figure 11**, we can see the E_c of the H_3-V system is 2.97 eV below the CBM, while the E_v remains the same. The H_3-V system exhibits 0.57 eV actual band gap energy. Surprisingly, the H_4-V system exhibits a similar band gap energy to that of the pure diamond, which is 3.90 eV (**Figure 12**). Therefore, it can be inferred that in the case of H_1-V, H_2-V and H_3-V, the H-interstitials act as deep donors which create additional states between CBM and Fermi levels. In consequence, the new states will promote electron mobility from the valence band into the conduction band which further improves the electronic property of the modified-diamond. In the case of H_4-V, the dangling bonds are completely passivated by the H-interstitials. Thus, its band gap energy is returned to the pure diamond. Likewise, both systems have T_d symmetry. Nevertheless, the volumetric sizes of both systems are completely different. As mentioned above, the H_4-V system is 48.70 % wider than the pure diamond. Likely, it is possible to obtain 2 different geometric systems with similar symmetries and electronic properties.

Conclusions

We have successfully demonstrated the effect of the complex carbon-vacancy-hydrogen defects on the pure diamond. The presence of the H-interstitials (H_1-V, H_2-V and H_3-V) changes the band structures, which is indicated by reducing the band gap and additional states near the Fermi level. Likely, the H-interstitials compensate for the C-monovacancy which further serves as a deep donor. More importantly, we discover unique properties of the H4-V system. H_4-V has a 48.70 % wider volumetric size compared to the pure diamond; however, it exhibits similar symmetry and band gap energy to that of the pure diamond.

Acknowledgements

The work is supported by "Penelitian Tesis Magister" research grant No. 122/E5/PG.02.00.PL/2023; 3218/UN1/DITLIT/Dit-Lit/PT.01.03/2023. The computations use the ALELEON Supercomputer at EFISON Lisan Teknologi HQ, Indonesia.

References

[1] A Chepurov, V Sonin, D Shcheglov, E Zhimulev, S Sitnikov, A Yelisseyev and A Chepurov. Surface Porosity of Natural Diamond Crystals after the Catalytic Hydrogenation. *Crystals* 2021; **11**, 1341.
[2] S Łoś, K Fabisiak, K Paprocki, M Szybowicz, A Dychalska, E Spychaj-Fabisiak and W Franków. The hydrogenation impact on electronic properties of p-diamond/n-Si heterojunctions. *Materials* 2021; **14**, 6616.
[3] H Gomez, MN Groves and MR Neupane. Study of the structural phase transition in diamond (100) & (111) surfaces. *Carbon Trends* 2011; **3**, 33.
[4] ZS Fatomi, AD Nugraheni and Sholihun. Vibrational effect on vacancy concentration in diamond: The density-functional-theory calculation. *Comput. Condens. Matter* 2022; **32**, e00708.
[5] Y Dai, CX Yan, AY Li, Y Zhang and SH Han. Effects of hydrogen on electronic properties of doped diamond. *Carbon* 2005; **43**, 1009-14.
[6] CJH Wort and RS Balmer. Diamond as an electronic material. *Mater. Today* 2008; **11**, 22-8.
[7] J Isberg, J Hammersberg, E Johansson, T Wikström, DJ Twitchen, AJ Whitehead, SE Coe and GA Scarsbrook. High carrier mobility in single-crystal plasma-deposited diamond. *Science* 2002; **297**, 1670-2.
[8] H Sakaue, N Yoshimura, S Shingubara and T Takahagi. Low dielectric constant porous diamond films formed by diamond nanoparticles. *Appl. Phys. Lett.* 2003; **83**, 2226-8.
[9] JP Goss, R Jones, MI Heggies, CP Ewels, PR Briddon and S Öberg. Theory of hydrogen in diamond. *Phys. Rev. B* 2002; **65**, 115207.
[10] D Purnawati, N Fajariah, H Prayogi, JP Bermundo, AD Nugraheni and Sholihun. Dissociation-energy calculations of C-multivacancies in diamond: The density-functional-theory study. *Jpn. J. Appl. Phys.* 2023; **62**, 051002.
[11] XJ Hu, YB Dai, RB Li, HS Shen and XC He. The diffusion of vacancies near a diamond (001) surface. *Solid State Comm.* 2002; **122**, 45-8.
[12] B Slepetz and M Kertesz. Divacancies in diamond: A stepwise formation mechanism. *Phys. Chem. Chem. Phys.* 2014; **16**, 1515-21.
[13] R Jones, LS Hounsome, N Fujita, S Öberg and PR Briddon. Electrical and optical properties of multivacancy centres in diamond. *Phys. Status Solidi* 2007; **204**, 3059-64.

[14] DP Hastuti, W Amalia, Z Priska, P Nurwantoro and Sholihun. First-principles density-functional-theory calculations of formation and dissociation energies in germanene multivacancies. *Mater. Today Comm.* 2020; **22**, 100754.
[15] M Saito, K Yamashita and T Oda. Magic numbers of graphene multivacancies. *Jpn. J. Appl. Phys.* 2007; **46**, L118.
[16] DP Hastuti, P Nurwantoro and Sholihun. Stability study of germanene vacancies: The first-principles calculations. *Mater. Today Comm.* 2018; **19**, 459-63.
[17] X Chang, Q Xue, D He, L Zhu, X Li and B Tao. 585 divacancy-defective germanene as a hydrogen separation membrane: A DFT study. *Int. J. Hydrogen Energ.* 2017; **42**, 24189-96.
[18] S Lebègue and O Eriksson. Electronic structure of two-dimensional crystals from ab initio theory. *Phys. Rev. B* 2009; **79**, 115409.
[19] K Takeda and K Shiraishi. Theoretical possibility of stage corrugation in Si and Ge analogs of graphite. *Phys. Rev. B* 1994; **50**, 14916.
[20] T Yamasaki, A Kuroda, T Kato, J Nara, J Koga, T Uda, K Minami and T Ohno. Multi-axis decomposition of density functional program for strong scaling up to 82,944 nodes on the K computer: Compactly folded 3D-FFT communicators in the 6D torus network. *Comput. Phys. Comm.* 2019; **244**, 264-76.
[21] Sholihun, W Amalia, DP Hastuti, P Nurwantoro, AD Nugraheni and RHS Budhi. Magic vacancy-numbers in h-BN multivacancies: The first-principles study. *Mater. Today Commun.* 2019; **20**, 100591.
[22] A Abdurrazaq, AT Raji and WE Meyer. Effect of isovalent doping on hydrogen passivated vacancy-oxygen defect complexes in silicon: Insight from density functional theory. *Silicon* 2021; **13**, 1969-77.
[23] JP Goss. Theory of hydrogen in diamond. *J. Phys. Condens. Matter.* 2003; **15**, R551.
[24] P Briddon, R Jones and GMS Lister. Hydrogen in diamond. *J. Phys. C Solid State Phys.* 1988; **21**, L1027.
[25] D Saada, J Adler and R Kalish. Lowest-energy site for hydrogen in diamond. *Phys. Rev. B* 2000; **61**, 10711.
[26] W Amalia, P Nurwantoro and Sholihun. Density-functional-theory calculations of structural and electronic properties of vacancies in monolayer hexagonal boron nitride (h-BN). *Comput. Condens. Matter* 2019; **16**, e00354.
[27] F Birch. Finite elastic strain of cubic crystals. *Phys. Rev.* 1947; **71**, 809.
[28] AK McMahan. Interstitial-sphere linear muffin-tin orbital structural calculations for C and Si. *Phys. Rev. B* 1984; **30**, 5835.
[29] MT Yin and ML Cohen. Ground-state properties of diamond. *Phys. Rev. B* 1981; **24**, 6121.
[30] W Kaiser and WL Bond. Nitrogen is a major impurity in common type I diamonds. *Phys. Rev.* 1959; **115**, 857.
[31] T Yamanaka, S Morimoto and H Kanda. Influence of the isotope ratio on the lattice constant of diamond. *Phys. Rev. B* 1994; **14**, 9341.
[32] H Holloway, KC Hass, MA Tamor, TR Anthony and WF Banholzer. Isotopic dependence of the lattice constant of diamond. *Phys. Rev. B* 1991; **13**, 7123.
[33] D Richards and M Amos. Shape optimization with surface-mapped CPPNs. *IEEE Trans. Evol. Comput.* 2016; **21**, 391-407.
[34] S Sholihun, HP Kadarisman and P Nurwantoro. Density-functional-theory calculations of formation energy of the nitrogen-doped diamond. *Indonesian J. Chem.* 2018; **18**, 749-54.
[35] Z Priska, S Hidayati, S Sholihun, W Amalia and P Nurwantoro. Hydrogen and water adsorptions on monolayer hexagonal boron nitride (h-BN): The first-principles calculations. *Key Eng. Mater.* 2021; **884**, 387-93.
[36] YN Apriati, AD Nugraheni and S Sholihun. Interaction of C_{60} with small molecules: Adsorption - inclusion energy calculation using the density functional theory. *Mater. Sci. Forum* 2022; **1066**, 135-43.
[37] C Glover, ME Newton, PM Martineau, S Quinn and DJ Twitchen. Hydrogen incorporation in diamond: The vacancy-hydrogen complex. *Phys. Rev. Lett.* 2004; **92**, 135502.
[38] DEP Vanpoucke and K Haenen. Revisiting the neutral C-vacancy in diamond: Localization of electrons through DFT+ U. *Diam. Relat. Mater.* 2017; **79**, 60-9.
[39] A Zelferino, S Salustro, J Baima, V Lacivita, R Orlando and R Dovesi. The electronic states of the neutral vacancy in diamond: A quantum mechanical approach. *Theor. Chem. Accounts Theor. Comput. Model. Theor. Chim. Acta* 2016; **135**, 74.

[40] AA Emery and C Wolverton. High-throughput DFT calculations of formation energy, stability and oxygen vacancy formation energy of ABO_3 perovskites. *Sci. Data* 2017; **4**, 170153.
[41] RQ Hood, PRC Kent, RJ Needs and PR Briddon. Quantum monte Carlo study of the optical and diffusive properties of the vacancy defect in diamond. *Phys. Rev. Lett.* 2003; **91**, 076403.
[42] K Ramakrishna and J Vorberger. Ab-initio dielectric response function of diamond and other relevant high-pressure phases of carbon. *J. Phys. Condens. Matter* 2019; **32**, 095401.
[43] P Deák, B Aradi, T Frauenheim, E Janzén and A Gali. Accurate defect levels were obtained from the HSE06 range-separated hybrid functional. *Phys. Rev. B* 2010; **81**, 153203.
[44] F Tran and P Blaha. Importance of the kinetic energy density for band gap calculations in solids with density functional theory. *J. Phys. Chem.* 2017; **121**, 3318-25.
[45] O Madelung. *Semiconductors-basic data*. Springer Book Archive. Springer Berlin, Heidelberg, Germany, 1996.
[46] SP Gao. Band gaps and dielectric functions of cubic and hexagonal diamond polytypes calculated by many-body perturbation theory. *Phys. Status Solidi B* 2015; **252**, 235-42.
[47] Y Ma, J Ma, Y Lv, J Liao, Y Ji and H Bai. Effect of mono vacancy defect on the charge carrier mobility of carbon nanotubes: A case study on (10,0) tube from first-principles. *Superlattice. Microst.* 2016; **99**, 140-4.